Phase Behavior of Aqueous Dispersions of Colloidal Boehmite Rods

P. A. Buining, A. P. Philipse, and H. N. W. Lekkerkerker*

Van't Hoff Laboratory, University of Utrecht, Padualaan 8, 3584 CH Utrecht, The Netherlands

Received July 30, 1993. In Final Form: March 9, 1994[⊗]

We report the phase behavior of aqueous dispersions containing rodlike boehmite particles with two different average lengths, 130 and 280 nm, with length-to-width ratios of approximately 8 and 20, over a range of ionic strengths. At low salt concentrations, where the particle interaction is predominantly repulsive, a separation into an isotropic upper phase and a birefringent lower phase occurs in the system containing the high-aspect-ratio particles. This phase separation was not observed in the case of dispersions containing the shorter particles. This seems to indicate that the phase separation is driven by the excluded volume effect. Above a critical (low) particle concentration, the repulsive 280 nm long rods form a monophasic birefringent glassy phase. This concentration is much lower than that at the isotropic–nematic transition as predicted from Onsager's theory for charged rods. Above a critical ionic strength a regime is entered where the phase behavior is largely governed by the attractive interaction. Then for both aspect ratios a space-filling amorphous gel is formed.

I. Introduction

The colloid-chemical behavior of dispersions of particles of anisometric shape is rich and varied. In a seminal paper, Langmuir[1] reported studies on both plate-shaped (bentonite) and rod-shaped colloids (tobacco mosaic virus and vanadium pentoxide). These systems exhibit, already at low volume fractions, interesting phenomena such as streaming birefringence, thixotropy, elasticity, and a phase separation into a birefringent, orientationally-ordered lower phase and an isotropic upper phase. Since then, these phenomena were also described for dispersions of other rodlike colloidal particles, such as boehmite (γ-AlOOH),[2,3] β-FeOOH,[4] cellulose microcrystals,[5,6] and poly(tetrafluoroethylene) "whiskers".[7]

According to the classical DLVO theory,[8,9] the stability of a dispersion of charged colloidal particles is a sensitive balance between repulsive interparticle forces, determined by electric-double-layer overlap, and attractive van der Waals forces. For nonspherical colloids this balance, and thus colloid stability, depends on the mutual particle orientation. In general, a division can be made into two stability regimes: (1) at low ionic strength a regime where repulsion dominates and (2) at high ionic strength a domination of attraction.

In the first regime, rodlike systems are expected to be stable dispersions but may show phase separation into a birefringent, orientationally-ordered lower phase and an isotropic upper phase. Langmuir[1] regarded the parallel ordered particles in the lower phase as held in lattice-like positions by strong repulsive interparticle forces, resulting from the charge on the particle surface. In the early 1940s, Onsager[10] explained the formation of the ordered nematic phase as driven by the excluded-volume effect. When the rods take up more or less parallel orientations, the excluded-volume contribution to the entropy can overrule the loss of orientational entropy of the system. Therefore, a phase with a preferred particle orientation can be the stable configuration. The phase separation takes place above a critical particle volume fraction, which depends for hard rods only on the aspect ratio of the particles.

In case the particles are charged, they can be treated in the Onsager approach as hard rods with an increased, effective diameter D_{eff}. This effective diameter, which is related to the particle surface potential and the Debye screening length κ^{-1} of the diffuse double layer, leads to an increased excluded-volume effect. Therefore, a dispersion of charged particles shows phase separation at a lower particle volume fraction than a bare hard-particle system. The Debye length varies inversely as the square root of the ionic strength. A decreasing salt concentration will shift the phase separation to a lower volume fraction. This effect was indeed found experimentally for the tobacco mosaic virus (TMV) system.[11] The formation of an ordered phase of charged rods is counteracted by the tendency of two charged parallel cylinders to rotate to a crossed orientation. It was shown by Stroobants et al.[12] that this effect is governed by the "twist" parameter $h = (\kappa D_{eff})^{-1}$.

In the case that so much salt is added that van der Waals attractive interparticle forces dominate, dispersions of rodlike colloidal particles have a strong tendency to form a space-filling isotropic gel.[6,13] Vold[14] predicted theoretically that the critical volume fraction for gelation decreases with increasing particle aspect ratio.

This study describes the phase behavior of a novel colloidal rodlike boehmite (γ-AlOOH) system in water. Dispersions containing particles with two different lengths (130 and 280 nm) were studied over a range of both salt and acid concentrations (10^{-4} to 1 M). Depending on the ionic strength, very dilute boehmite dispersions show either phase separation or gelation. On increasing the particle concentration, the low-salt-containing 280 nm rod dispersion becomes a viscoelastic birefringent glassy phase

⊗ Abstract published in *Advance ACS Abstracts*, June 1, 1994.

(1) Langmuir, I. *J. Chem. Phys.* **1938**, *6*, 873.
(2) Zocher, H.; Török, C. *Kolloid Z.* **1960**, *170*, 140; **1960**, *173*; 1; **1962**, *180*, 41.
(3) Bugosh, J. *J. Phys. Chem.* **1961**, *65*, 1789.
(4) Maeda, Y.; Hachisu, S. *Colloids Surf.* **1983**, *6*, 1.
(5) Marchessault, R. H.; Morehead, F. F.; Walter, N. M. *Nature* **1959**, *184*, 632.
(6) Hermans, J. *J. Polym. Sci.* **1963**, *C2*, 129.
(7) Folda, T.; Hoffmann, H.; Chanzy, H.; Smith, P. *Nature* **1988**, *333*, 55.
(8) Deryagin, B. V.; Landau, L. *Acta Physicochim. URSS* **1941**, *14*, 633.
(9) Verwey, E. J. W.; Overbeek, J. Th.G. *Theory of the Stability of Lyophobic Colloids*; Elsevier: Amsterdam, The Netherlands, 1948.
(10) Onsager, L. *Ann. N.Y. Acad. Sci.* **1949**, *51*, 627.
(11) Fraden, S.; Maret, G.; Caspar, D. L. D.; Meyer, R. B. *Phys. Rev. Lett.* **1989**, *63*, 2068.
(12) Stroobants, A.; Lekkerkerker, H. N. W.; Odijk, T. *Macromolecules* **1986**, *19*, 2232.
(13) Buscall, R. *Colloids Surf.* **1982**, *5*, 269.
(14) Vold, M. J. *J. Phys. Chem.* **1959**, *63*, 1608.

0743-7463/94/2410-2106$04.50/0 © 1994 American Chemical Society

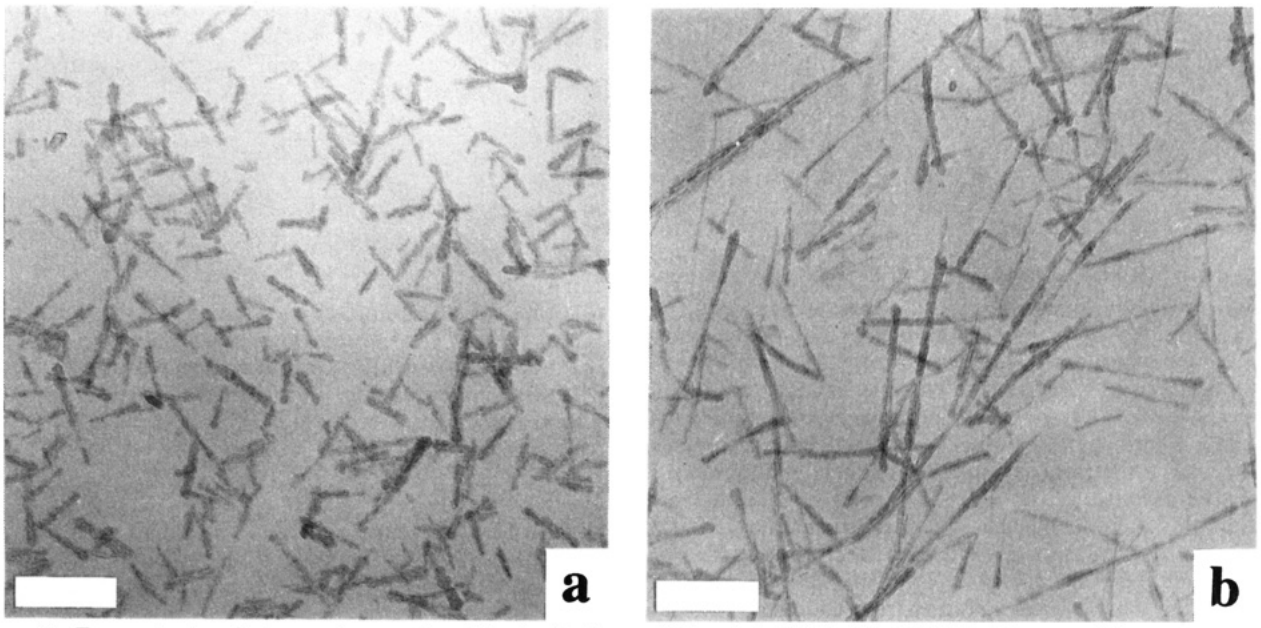

Figure 1. Transmission electron micrographs of the boehmite particles: (a) ASB31; (b) ASBIP8. Bars are 0.2 μm.

at boehmite concentrations above 0.7 wt %. To correlate all these phenomena with the ionic-strength range, calculations for the interaction energies between two cylindrical particles in parallel as well as in crossed orientation are presented. The particle volume fraction which marks the onset of the birefringent glassy phase is compared with the volume fraction at which a nematic monophase should form according to Onsager's theory of the isotropic–nematic (I–N) phase transition for charged rods.[12]

The boehmite rod size and shape were determined by transmission electron microscopy. The boehmite surface was characterized by measurement of the surface-charge density and the surface potential using potentiometric titration and electrophoresis, respectively. Also, the isoelectric point (iep) was determined.

II. Sample Preparation

The boehmite dispersions were prepared as described earlier[15] by hydrothermal treatment of an aqueous aluminum-alkoxide mixture, acidified with hydrochloric acid. The dispersions prepared for this study, coded ASB31 and ASBIP8, have two different average rod lengths, about 130 and 280 nm, respectively. Immediately after preparation, the dispersions were purified of alcohol (produced during synthesis) and chloride by dialysis in a cellophane tube against demineralized water for 1 week at room temperature. During dialysis, the pH of both dispersions increased from about 1 to about 4.3. The HCl concentrations (c_{HCl}) after dialysis were calculated from measured conductivities (K_{HCl}) of the dispersion, according to

$$c_{HCl} = K_{HCl}/\Lambda_{0,HCl} \quad (1)$$

with $\Lambda_{0,HCl}$ the specific conductivity of HCl. K_{HCl} was measured with the same PEN KEM 3000 system as was used for the electrokinetic measurements. The dispersions were stored in poly(ethylene) containers to avoid adsorption of silicates from glassware on the boehmite surface.

The dispersion ASBIP8 (long rods) shows streaming birefringence above a concentration of boehmite of 0.017 wt %. Above 0.67 wt % the dispersion is permanently birefringent (see section IV). The dispersion ASB31 (short rods) shows streaming birefringence above $w \approx 0.41$ wt %. The salt-containing dispersions were prepared by adding a NaCl solution to the dialyzed dispersion under stirring, after which the dispersion was sonicated for a few minutes.

For stability tests, a series of test tubes were filled with identical amounts of the start dispersions ASB31 and ASBIP8 with boehmite concentrations of 1.07 and 0.87 wt %, respectively. To these dispersions equal portions (twice the volume of the original dispersion) of HCl or NaCl solutions of rising concentration were added. This procedure leads to final boehmite concentrations of 0.36 wt % (ASB31) and 0.29 wt % (ASBIP8) and of NaCl or HCl ranging from 10^{-4} to 1 M. The dispersions were subsequently sonicated for a few minutes and left undisturbed at room temperature for 10 months. For study at higher boehmite concentrations, both (dialyzed) dispersions were slowly concentrated by stirring them for a few days in the open air at about 70 °C. By this procedure, ASBIP8 was concentrated up to 6.7 wt % and ASB31 up to 10 wt %.

Table 1. Characterization Results of Dialyzed Boehmite Dispersions

	ASB31	ASBIP8
L_{av}/nm	130	281
s_L/nm	44	132
D_{av}/nm	17	14
s_D/nm	4	3
$K/10^{-3}$ S m^{-1}	2.95	4.15
$c_{HCl}/10^{-5}$ M	6.92	9.77
κ^{-1}/nm	36.6	30.8
$\phi_d/10^{-3}$ V[a]		~75
$\phi_0/10^{-3}$ V[b]	~130	
σ_0/C m^{-2} [c]	0.11	
proton density/nm^{-2} [c]	0.71	
iep	9.8	
S_{spec}/m^2 g^{-1}	184	225

[a] pH = 5. [b] pH $\lesssim$ 7.6. [c] pH = 3.2.

III. Characterization

Electron Microscopy. The TEM specimens were prepared by spraying the boehmite dispersion with a nebulizer onto a formfar-coated carrier grid. The grid was placed in a CM-10 Philips transmission electron microscope. Electron micrographs of dispersions ASB31 and ASBIP8 are shown in Figure 1. The average particle lengths (as determined from the micrographs) are given in Table 1. The rods have a flattened shape with a width as given in Table 1 and a thickness of invariably about 8 nm.[15]

Background of Electrophoresis. At the boehmite surface, the –AlOH groups may be ionized according to

(15) Buining, P. A.; Pathmamanoharan, C.; Jansen, J. B. H.; Lekkerkerker, H. N. W. *J. Am. Ceram. Soc.* **1991**, *74*, 1303.

the following reactions[16]

$$-AlOH_2^+ \rightleftharpoons -AlOH + H^+(aq);$$

$$K_{a1} = \frac{\Gamma_{AlOH}[H^+]}{\Gamma_{AlOH_2^+}} \exp\left(\frac{-e\psi_0}{kT}\right) \quad (2)$$

$$-AlOH \rightleftharpoons -AlO^- + H^+(aq);$$

$$K_{a2} = \frac{\Gamma_{AlO^-}[H^+]}{\Gamma_{AlOH}} \exp\left(\frac{-e\psi_0}{kT}\right) \quad (3)$$

where Γ represents a surface concentration and e the proton charge. According to the site-binding model[16,17] the centers of the charged surface ions ($-O^-$, $-OH_2^+$) are located in the surface plane having potential ψ_0. Onto this plane, unhydrated counterions (e.g. Cl^-) may adsorb, and their centers are located in the so-called inner Helmholtz plane (IHP). The outer Helmholtz plane (OHP) is the closest distance of approach of free, hydrated counterions to the surface of boehmite. Thus, the diffuse part of the double layer extends from the OHP into the solution.

By combining the equilibrium constants (eqs 2 and 3) and by noting that the point of zero charge can be expressed by pzc = $^1/_2(pK_{a1} + pK_{a2})$, we get

$$\psi_0 = \frac{(\ln 10)kT}{e}\left[pzc - pH + \frac{1}{2}\log\left(\frac{\Gamma_{AlO^-}}{\Gamma_{AlOH_2^+}}\right)\right] \quad (4)$$

which can be used to determine ψ_0 as a linear function of pH when the pzc is known and the logarithmic term is negligible. Near the pzc this negligibility is justified, because then the concentration ratio in eq 4 is near unity. In calculating ψ_0, we assume that only minor counterion adsorption takes place in the vicinity of the pzc[18] and therefore approximate the pzc by the iep, which is determined by electrokinetic measurement.

What we measure as ζ-potential is in fact the potential at the slipping plane. Usually in electrophoresis, this plane is assumed to coincide with the OHP (with potential ψ_d). To calculate ζ-potential values from the measured electrophoretic mobilities, we follow the approach of Henry[19] who, neglecting the relaxation effect, solved the hydrodynamic equations for *infinitely* long rods moving parallel or perpendicular to the applied electric field. For parallel movement, Smoluchowski's equation[20] applies, because the electric field is everywhere parallel to the particle surface. The relation between the electrophoretic mobility $\mu_{\parallel}$ and the ζ-potential, which is defined as the potential at the slipping plane, is

$$\mu_{\parallel} = \frac{u_{\parallel}}{E} = \frac{\epsilon_0\epsilon_r\zeta}{\eta_s}; \qquad \text{all } \kappa a \quad (5)$$

Here, $u_{\parallel}$ is the particle velocity, E the field strength, ϵ_0 the permittivity in vacuum, ϵ_r the relative permittivity of the solvent, η_s the solvent viscosity, κ the reciprocal Debye length, and a the cylinder radius.

For movement perpendicular to the applied field, the local field around the cylinder is distorted. Henry's numerical results for the mobility now depend on κa. At high and low κa these results reduce, respectively, to the Smoluchowski equation and half that equation

$$\mu_{\perp} = \frac{\epsilon_0\epsilon_r\zeta}{\eta_s}; \qquad \kappa a \gg 1 \quad (6)$$

$$\mu_{\perp} = \frac{\epsilon_0\epsilon_r\zeta}{2\eta_s}; \qquad \kappa a < 1 \quad (7)$$

The relaxation effect was found by Wiersema et al.[21] and Stigter[22] to be indeed negligible at high and low κa at all ζ-potentials, and at intermediate κa for low ζ-potential only. For high ζ-potential and intermediate κa (roughly between 2 and 50) the relaxation effect leads to a mobility which is nearly independent of ζ. Interpretation of electrophoresis data is then virtually impossible.

De Keizer et al.[23] have shown that in a dilute system of freely diffusing cylinders the mobility of a cylinder, averaged over all particle orientations, can be expressed as

$$\bar{\mu} = \frac{1}{3}\mu_{\parallel} + \frac{2}{3}\mu_{\perp} \quad (8)$$

It is assumed here that particles are not oriented by the electric field while they move through the solvent. In conclusion, at $\kappa a < 1$ the relaxation effect may be neglected and by combining eqs 5–8, the average mobility for *infinitely* long rods is found to be

$$\bar{\mu} = \frac{2\epsilon_0\epsilon_r\zeta}{3\eta_s}; \qquad \kappa a < 1 \quad (9)$$

Note that this expression equals the Hückel equation for the electrophoretic mobility of a sphere,[24] which also applies at $\kappa a < 1$. Thus, for $\kappa a < 1$ the average mobility of a very long cylinder equals that of a sphere with the same radius and ζ-potential.

Electrokinetic Measurements. Electrophoretic mobilities were measured at 25 °C with a PEN KEM SYSTEM 3000 automated electrokinetics analyzer, a laser-doppler apparatus which determines the particle velocity at the stationary solvent layers. The experimental error of this apparatus is less than 2%. To apply eq 9, valid in the case of a thick double layer, the electrophoretic mobility was measured of the high-aspect-ratio rods of ASBIP8 at a low particle concentration (w = 0.032 wt %) and low ionic strength ($K = 3.4 \times 10^{-4}$ S m^{-1}, κ^{-1} = 107 nm). This was achieved by diluting the dialyzed ASBIP8 system with twice-distilled water (final pH ≈ 5). The very low particle volume fraction reduces the chance of double-layer interaction at this large κ^{-1}. The measured mobility of $(4.1 \pm 0.5) \times 10^{-8}$ m^2 V^{-1} s^{-1} corresponds according to eq 9 with a ζ-potential of about 75 mV (see also Table 1). At the very low electrolyte concentration, counterion adsorption is low, and the potential at the OHP, ψ_d, approximated by the measured ζ-potential, will most closely approach ψ_0.

To measure the mobility as a function of pH, small portions of a 1.00 M NaOH solution were added stepwise under vigorous stirring to a 0.357 wt % ASB31 dispersion,

(16) Davis, J. A.; James, R. O.; Leckie, J. O. *J. Colloid Interface Sci.* **1978**, *63*, 480; **1978**, *67*, 90.
(17) Yates, D. E.; Levine, S.; Healy, T. W. *J. Chem. Soc., Faraday Trans. 1* **1974**, *70*, 1807.
(18) Kallay, N.; Tomić, M. *Langmuir* **1988**, *4*, 559.
(19) Henry, D. C. *Proc. R. Soc. London* **1931**, *A133*, 106.
(20) Smoluchowski, M. In *Handbuch der Elektrizität und des Magnetismus*; Graetz, L., Ed.; Barth: Leipzig, 1921; Vol. II, p 366.
(21) Wiersema, P. H.; Loeb, A. L.; Overbeek, J. Th. G. *J. Colloid Interface Sci.* **1966**, *22*, 78.
(22) Stigter, D. *Biopolymers* **1977**, *16*, 1415.
(23) Keizer, A. de; van der Drift, W. P. J. T.; Overbeek, J. Th. G. *Biophys. Chem.* **1975**, *3*, 107.
(24) Hückel, E. *Phys. Z.* **1924**, *25*, 204.

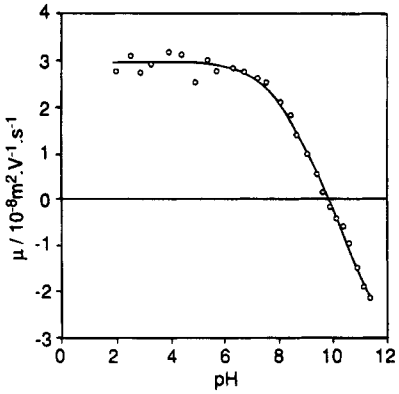

Figure 2. Electrophoretic mobility of the ASB31 dispersion (0.36 wt %) as a function of pH, obtained by addition of 1.00 M NaOH.

which was previously brought to pH = 2 by adding a 1 M HCl solution. The pH measurements were performed using a glass electrode. The added NaOH portions corresponded to successive pH increments of about 0.5 and are small enough to keep the boehmite concentration virtually constant. A few minutes after each addition the electrophoretic mobility was measured (Figure 2). From pH 2 to 7.6 the constant mobility indicates that the surface is "saturated" with $-AlOH_2^+$ groups and that H^+ ions do not influence the surface potential. In the region from pH 7.6 to 11.2, the ζ-potential, and with that the potential ψ_d at the OHP, depends almost linearly on pH. This means that no adsorption of Cl^- ions occurs in a broad pH range around the pzc, because ion adsorption would give a clear deviation from linearity.[25] Consequently, the iep approaches the pzc value. The iep is found to occur at a pH of 9.8. By comparison, Wood et al.[26] found an iep of 9.1 for boehmite in a KNO_3 solution. Further, from Huang's experimental pK_{a1} and pK_{a2} values[27] we find a pzc of 8.6.

The surface potential ψ_0 was calculated using eq 4 with pH ≈ 7.6 as the pH value beyond which ψ_0 has its maximum "saturation" value. The resulting $\psi_0 \approx 130$ mV (see also Table 1) appears to be much larger than the estimated ψ_d (≈75 mV). This is not unusual; especially in the case of adsorbed Cl^- ions in the IHP, the potential is known to drop dramatically over the triple layer.[16] The wide variety in the iep and pzc values of aluminum oxide or hydroxide surfaces found in the literature can be ascribed to several factors. Alumina surfaces seem to reach equilibrium quite slowly when subjected to changes of pH or ionic strength. The pzc may also be lowered by adsorption of atmospheric CO_2, as described by Zeltner et al.[28] for the FeOOH surface.

A comparison of our electrophoresis results with those of Ramsay et al.[29] for dispersions of platelike boehmite particles (about 25 nm across and 4 nm thick) reveals many similarities. They found a mobility of $(4 \pm 0.5) \times 10^{-8}\,m^2\,s^{-1}\,V^{-1}$ at pH = 4, in agreement with our findings. Ramsay et al. also observed that the mobility hardly changed in the pH range from 3 to 6, but decreased at pH > 6, to give an iep between 8 and 9.

Potentiometric Titration. The potentiometric titration was performed by adding a 1.62 mM NaOH solution in portions to 80 mL of a 0.535 wt % ASB31 dispersion,

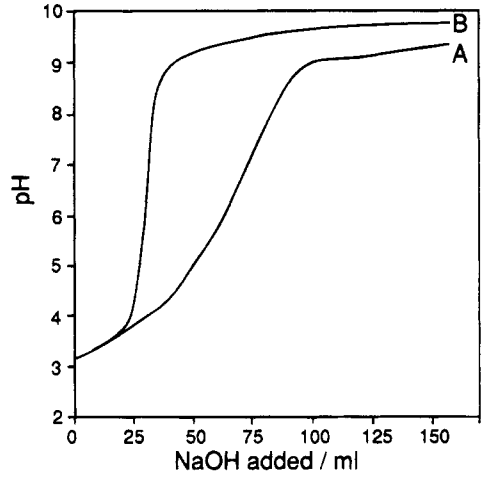

Figure 3. Potentiometric titration by adding 1.62 mM NaOH to 80 mL of ASB31 dispersion (0.54 wt %) with start-pH 3.2 (curve A). As a reference an equivalent titration was performed on a HCl solution with start pH 3.2 (curve B).

which was brought to pH = 3.2 previously by adding HCl solution. A HCl solution with a pH of 3.2, subjected to the same procedure, served as reference. After each NaOH addition the dispersion was allowed to equilibrate for a few minutes to a constant pH. Upon NaOH addition, the boehmite dispersion consumes an excess amount of NaOH compared to the reference HCl solution in reaching the same pH. The reason is that the boehmite dispersion uses some NaOH to neutralize acid $-AlOH_2^+$ groups on the boehmite surface. Consequently, the total excess amount of NaOH added when the pH reaches the pzc (about the iep) equals the amount of $-AlOH_2^+$ groups present on the surface at the start pH of 3.2. The potentiometric titrations of both the dispersion and the HCl reference are plotted in Figure 3.

The surface charge per area on the boehmite particle can then be calculated according to

$$\sigma_0 = \frac{n_{NaOH}F}{wVS_{spec}} \tag{10}$$

where n_{NaOH} is the molar amount of NaOH added until pH = pzc, F is the Faraday constant, w is the weight concentration boehmite, V is the starting volume of dispersion, and S_{spec} is the specific surface area of the boehmite of ASB31 ($184\,m^2\,g^{-1}$, as determined by nitrogen adsorption of freeze-dried ASB31). The value of σ_0 calculated this way (see Table 1) gives a corresponding net proton density of 0.71 sites nm^{-2}. This value is lower than the maximum hydroxyl-site density found in literature (9 (OH) nm^{-2} for γ-AlOOH[26] and 8 (OH) nm^{-2} for γ-Al_2O_3[30]). This would mean that only about 8% of the surface-hydroxyl groups are carrying a proton charge.

IV. Observations on Phase Behavior

Dominating Repulsive Interactions. Figure 4 summarizes the results of visual inspection of the samples over a period of 10 months. For NaCl or HCl concentrations below about 0.05 M, the dispersions containing the shorter particles (ASB31, w = 0.36 wt %, ϕ = 0.12 vol %) remain monophasic, even after a period of 1 year. However, for the same NaCl or HCl concentration range, the dispersions containing the longer particles (ASBIP8, w = 0.29 wt %, ϕ = 0.10 vol %) phase separate into a dense phase on the bottom and a dilute phase above it. The phase separation becomes visible to the naked eye in about

(25) Sprycha, R. *J. Colloid Interface Sci.* **1989**, *127* (1), 12.
(26) Wood, R.; Fornasiero, D.; Ralston, J. *Colloids Surf.* **1990**, *51*, 389.
(27) Huang, C. P. The Chemistry of the Aluminum Oxide-Electrolyte Interface; Ph.D. Thesis, Harvard University, 1971.
(28) Zeltner, W. A.; Anderson, M. A. *Langmuir* **1988**, *4*, 469.
(29) Ramsay, J. D. F.; Daish, S. R.; Wright, C. J. *Discuss. Faraday Soc.* **1978**, *65*, 65.
(30) Peri, J. B. *J. Phys. Chem.* **1965**, *69*, 211.

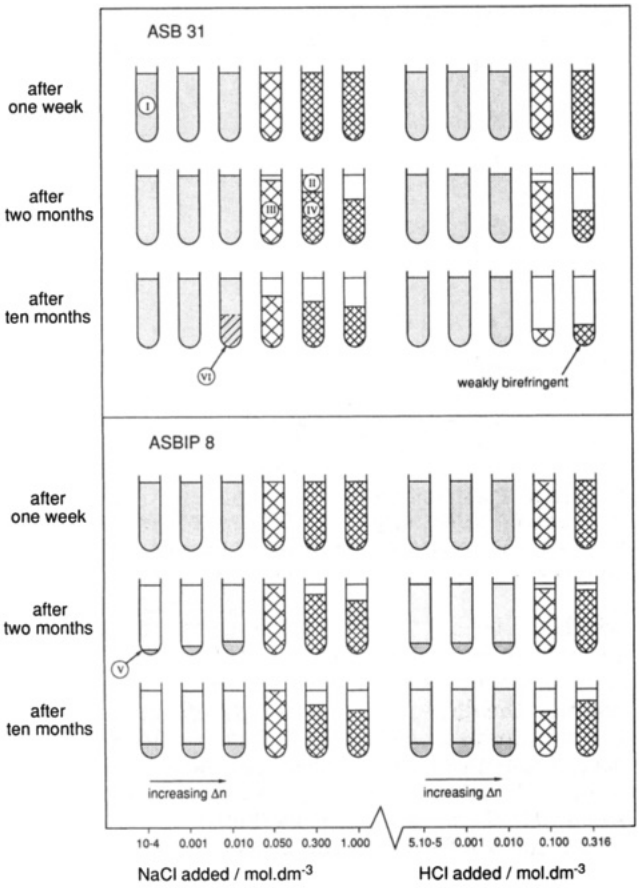

Figure 4. Stability tests on dispersions ASB31 (0.36 wt %) and ASBIP8 (0.29 wt %) done at various NaCl and HCl concentrations. I represents the dilute dispersion, II the supernatant, III a turbid space-filling isotropic gel of low viscosity, IV a turbid space-filling isotropic gel of high viscosity, V a highly viscous permanently birefringent phase, and VI a slightly turbid settled layer.

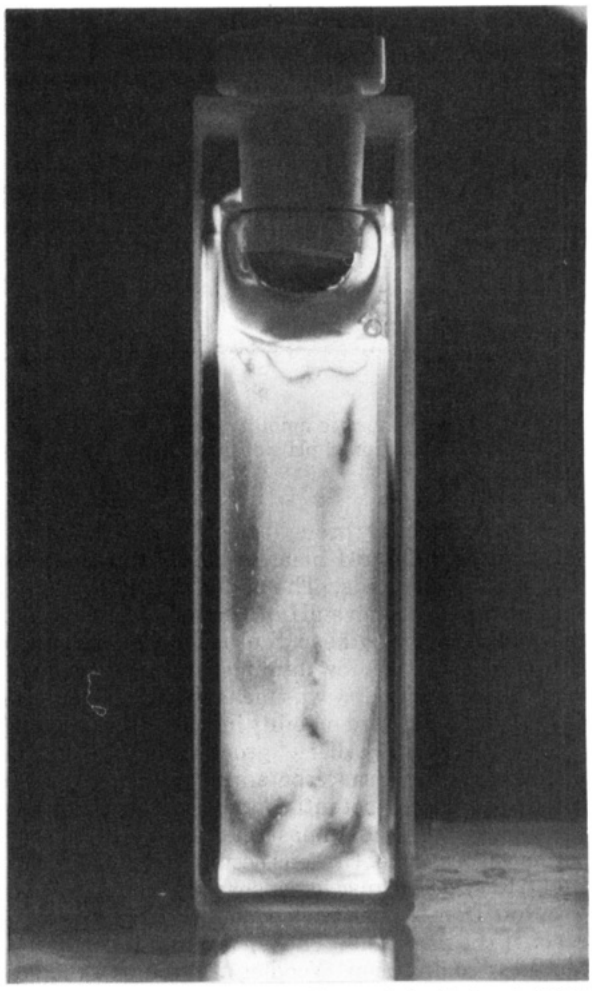

Figure 5. Birefringent glassy phase of the dialyzed ASBIP8 dispersion (0.9 wt %), placed between crossed polars.

1 month. When observed between crossed polaroids, the complete lower phase exhibits a permanent birefringence. This birefringence becomes more pronounced at increasing ionic strength. The lower phase is viscous and does not flow upon tilting the tube. But when the tube is shaken, the whole system is homogenized quite easily and an isotropic dispersion results. This dispersion again phase separates with time. Transmission electron micrographs did not reveal a significant difference in particle size in the upper and lower phases.

The dispersions show no real difference in phase behavior whether NaCl or HCl is added. The HCl just acts as an indifferent electrolyte at pH values below 4.3, which was indeed concluded from the electrokinetic measurements.

In order to learn more about the phase separation that occurs in the ASBIP8 system at low ionic strength, systems with different boehmite concentrations were studied. When the boehmite volume fraction is increased, the coexisting birefringent-lower-phase to isotropic-upper-phase volume ratio increases. At a boehmite weight concentration above 0.67 wt % (hereafter referred to as w_a) or higher, the dialyzed ASBIP8 system turns into a permanently-birefringent monophasic dispersion (see Figure 5) with a high zero-shear viscosity. Remarkably this dispersion flows quite easily upon tilting the tube, in contrast to the behavior of the birefringent lower phase in the case of coexisting phases.

The behavior of air bubbles that enter the fully-birefringent dispersion after vigorous shaking was used to gain insight in the mechanical strength of the dispersion structure at rest. At first impression, small bubbles seem to be immobilized in the dispersion structure. It appears, however, that even the smallest visible bubbles slowly rise on a time scale of hours and even up to days. Between crossed polaroids, the dispersion shows a schlieren-like pattern of large areas of permanent birefringence that becomes frozen-in when the shaking is stopped. These large areas consist themselves of a "cross-hatched"-like pattern of much smaller domains. When the tube is slightly oscillated by hand, the whole structure (including the remaining bubbles) oscillates around its initial state. This indicates a strong elastic component in the structure. This type of dispersion can be seen as a "birefringent glass phase", as will be explained later.

At a much higher boehmite concentration of $w = 6.7$ wt %, the ASBIP8 birefringent glassy phase becomes extremely stiff. The tube can be turned upside down without any flow. Here, the small air bubbles stay trapped in the dispersion. Figure 6 shows this dispersion observed under the polarization microscope. The striated banding of different extinction is a typical frozen-in shear structure. The structure is built up of small domains each of which showing a particular birefringence, which extinguishes under either positive or negative (identical) angles with the initial direction of shear. When the dispersion is then "sheared" by lateral movement of the cover slip, the texture seems to be refined and the dispersion shows a more homogeneously-distributed birefringence coloring. Then, slowly the domains increase in size and again the criss-cross banded texture appears.

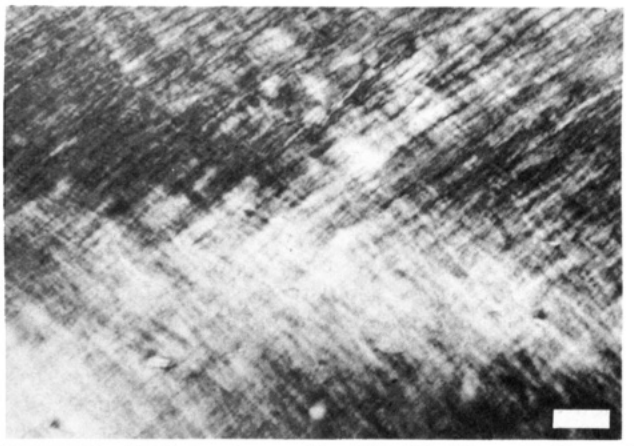

Figure 6. Optical micrograph of the birefringent phase of dispersion ASBIP8 (6.7 wt %) between crossed polars. Bar is 50 μm.

When to the birefringent ASBIP8 glassy phase of 0.9 wt % an amount of NaCl is added up to 0.01 M, a phase separation is observed with time. Immediately after the salt addition the whole dispersion becomes isotropic at rest, more turbid, and markedly less viscous. Within 2 months, a separation takes place into a lower stiff phase which is turbid, but strongly birefringent, and a transparent dispersion above it which is isotropic at rest. The lower phase exhibits a very fine pattern of birefringent domains (smaller than 0.5 mm). This phase is elastic; when subjected to small disturbances, its structure is not distorted but oscillates. When the tube is tilted, the lower phase does not flow because of its very rigid structure. The isotropic phase above it flows quite easily and exhibits streaming birefringence already under extremely slight movements.

The dialyzed ASB31 dispersion turns into a permanently-birefringent viscous glassy phase at a boehmite concentration of about 10 wt %, much higher than that of the ASBIP8 dispersion. This extremely stiff birefringent ASB31 glassy phase exhibits "ringing-gel" behavior, that is, a strong resonance response of the dispersion structure. When the ionic strength of the ASB31 glassy phase is increased, its viscosity drops but it remains monophasic, that is, it does not show phase separation in time.

Dominating Attractive Interactions. The stability tests (Figure 4) indicate that above a NaCl or HCl concentration between 0.05 and 0.10 M, both the diluted ASBIP8 and ASB31 sols turn irreversibly into space-filling gels, which are amorphous and very turbid. Within months the gels contract, leaving a clear supernatant. The ASB31 dispersion exhibits a higher contraction rate than ASBIP8. After densification to about 30% of its initial volume, the ASB31 gel has become weakly birefringent.

V. Discussion

Energy Calculations. The experiments indicate that at an ionic strength between 0.01 and 0.05 M the net interaction changes from repulsive to attractive. To verify whether this transition can be understood in terms of the DLVO theory, we calculated for these two ionic strengths the repulsive energy due to electric-double-layer overlap (V_R) and the van der Waals attractive energy (V_A), both for parallel (V^P) and crossed rods (V^C). For this purpose we used the expressions derived by Sparnaay[31] for the interaction between two cylinder-shaped colloidal particles.

We recapitulate here Sparnaay's expressions for the interaction energies between charged cylindrical particles of length L and radius a, surrounded by a double layer of 1:1 electrolyte. For arbitrary surface potentials (ψ_0) under the constraint of large κa, the repulsive energies due to double-layer overlap for parallel (V_R^P) and crossed cylinders (V_R^C) are respectively given by the expressions

$$V_R^P = 64(\pi)^{1/2}\, nkT\, \gamma^2\, L\, \frac{(\kappa a)^{1/2}}{\kappa^2} \exp(-\kappa H_0) \qquad (11)$$

$$V_R^C = 128\, \pi\, nkT\, \gamma^2\, \frac{a}{\kappa^2} \exp(-\kappa H_0) \qquad (12)$$

with

$$\gamma = \tanh\left(\frac{e\psi_0}{4kT}\right) \qquad (13)$$

In these equations, n is the number density of ions in the solution and H_0 is the surface-to-surface distance between the cylinders. It was noticed earlier by Stigter[32] that in the expression for V_R^C given by Sparnaay (eq 2.41 in ref 31) the factor π was accidently omitted.

The expression for the van der Waals attractive energy between parallel cylinders is

$$V_A^P = -\frac{3\pi}{8} A \frac{L}{a} a^5 U_5 \qquad (14)$$

where A is the Hamaker constant and U_5 is a rather complicated function of the cylinder radius, a, and the distance between the cylinder axes, R. In calculating V_A^P, the expression for U_5 is difficult to handle. For practical purposes Sparnaay introduces U_5 as a series in a/R

$$U_5 = \frac{1}{R^5}\left\{1 + 6.25\left(\frac{a}{R}\right)^2 + 31.90\left(\frac{a}{R}\right)^4 + 150.7\left(\frac{a}{R}\right)^6 + 684\left(\frac{a}{R}\right)^8 + 2200\left(\frac{a}{R}\right)^{10} + \ldots\right\} \qquad (15)$$

For short interparticle distances (say, $H_0 < a/2$) this expansion cannot be used. Sparnaay derived the following expression, valid for $H_0 \ll a$

$$V_A^P = -\frac{A}{24}\frac{L}{a}\left(\frac{a}{H_0}\right)^{3/2}\left(1 - \frac{9}{8}\frac{H_0}{a}\right) \qquad (16)$$

The last term in this equation was erroneously presented by Sparnaay (in his eq 3.11 in ref 31) as $9/8 \cdot (a/H_0)$.

The expression for the van der Waals attractive energy between crossed cylinders is

$$V_A^C = -\frac{A}{3}\left[\frac{1 - \frac{1}{2}k^2}{1 - k^2} E(k) - K(k)\right] \qquad (17)$$

where

$$k = 2a/R \qquad (18)$$

The functions E and K are the complete elliptic intergrals of, respectively, the first and second kind.

For the ionic strengths in our case, $I = 0.010$ M and $I = 0.050$ M, the corresponding κa values for the rods of ASBIP8 ($\kappa a = 2.3$ and $\kappa a = 5.0$) seem large enough for the eqs 11 and 12 for V_R^P and V_R^C to be valid. V_A^C was calculated from eq 17 using standard tables of elliptical intergrals.[33] Equation 16 and eq 14 (with eq 15) for V_A^P were used for short ($H_0/a < 0.5$) and long ($H_0/a > 0.5$) separations, respectively. The crossover distance $H_0/a =$

(31) Sparnaay, M. J. *Recl. Trav. Chim. Pays-Bas* **1959**, *78*, 680.

(32) Stigter, D. *Biopolymers* **1977**, *16*, 1435.

(33) *Handbook of Mathematical Functions*; Abramowitz, M., Stegun, I. A., Eds.; Dover Publications, Inc.: New York, 1968; p 587.

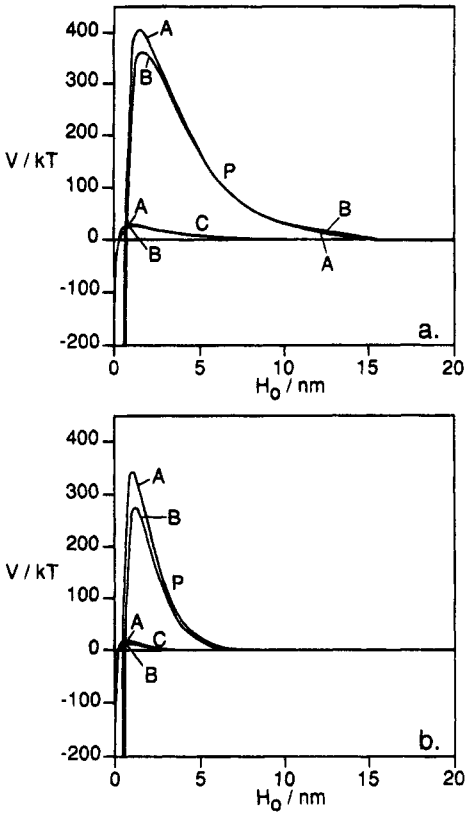

Figure 7. The energy of interaction $V = V_R + V_A$ between two cylindrical particles in parallel (P) and in crossed (C) orientation: (a) $\kappa^{-1} = 3.0$ nm; (b) $\kappa^{-1} = 1.4$ nm. Calculations performed for particle dimensions as in the ASBIP8 system and a surface potential $\psi_0 = 70$ mV: curves A, $A = 5.3 \times 10^{-20}$ J; curves B, $A = 6.7 \times 10^{-20}$ J.

0.5 was chosen because at this distance the attraction energies obtained from the expressions for short and large separation closely agree.

In all calculations we used a value of 70 mV for the surface potential, which equals the value of the ζ-potential determined by electrophoresis. For the Hamaker constant we used two different values reported in the literature for the mixed Hamaker constant of the crystalline-Al_2O_3 in water system, which we expect to approximate the values of crystalline-AlOOH in water. The first ($A = 5.3 \times 10^{-20}$ J), was calculated from dielectric properties,[34] the second ($A = 6.7 \times 10^{-20}$ J) was determined experimentally.[35,36]

In Figure 7 the total free energy of interaction ($V^{P,C} = (V_R + V_A)^{P,C}$) is plotted for two cylindrical particles with the average dimensions of ASBIP8 (length 280 nm and width 14 nm). Both parts a ($I = 0.010$ M) and b ($I = 0.050$ M) of Figure 7 show a large repulsive maximum in V^P and a much smaller maximum in V^C. It is therefore clear that in parallel orientation, the rods are stable at both ionic strengths. In crossed orientation, the maxima in V^C for $I = 0.010$ M are $30kT$ for the theoretical A and $27kT$ in case of the experimental A. For $I = 0.050$ M the maxima in V^C are lower, that is $17kT$ and $14kT$, respectively. This lowering may indeed herald the incipient crossover from repulsion dominated to attraction dominated, which is observed experimentally.

In the attractive regime, a parallel coagulation would seem favorable from Figure 7b, because this is the lowest-energy configuration. However, in case the rods coagulate very rapidly, they might follow the V^C curve to form disordered flocks.

The repulsive maxima in V^C are situated at distances between the particle surfaces of the order of 1 to 2 nm. At these short distances, non-DLVO forces like hydration forces are known to become effective. The boehmite surface, which contains strongly H-bonding hydroxyl groups, is expected to form an adjacent structured network of H-bonded water molecules, giving rise to hydration forces.[37] Due to these repulsive forces, the DLVO concept that we used in explaining colloid stability might not be fully applicable.

Dominating Repulsive Interactions. It is clear from Figure 4 that below an ionic strength of 0.01 M the ASBIP8 system of high aspect ratio rods shows phase separation. According to the energy calculations presented in the previous paragraph, we are dealing here with predominantly repulsive interactions resulting in a system of nonaggregated rods.

Increasing the particle concentration of the ASBIP8 dispersion (long rods), starting with a very low concentration (isotropic) and a low ionic strength (dialyzed, $I \approx 10^{-4}$ M), shows the following trajectories in the concentration, where the dispersion shows different behavior.

***w* < *w**.** Below a boehmite weight concentration w^* ($\approx$0.017 wt %) the dispersion is isotropic both at rest and when shaken. Apparently, more-particle double-layer interactions are insignificant in this concentration regime.

***w** < *w* < *w*$_a$.** The dispersion is isotropic at rest but shows streaming birefringence when disturbed. Its viscosity increases rapidly with particle concentration. These properties are determined by more-particle double-layer interactions. The phase separation at $w < w_a$ into an ordered lower phase and an isotropic upper phase seems to be driven by an excluded-volume effect. A strong indication for the occurrence of this effect is the absence of phase separation in the ASB31 system of low-aspect-ratio rods. At increasing ionic strength, the excluded volume decreases and the lower phase of ASBIP8 becomes more densely packed, as expressed by an increasing birefringence (see Figure 4). With increasing boehmite weight concentration the anisotropic-phase to isotropic-phase volume ratio increases.

***w* > *w*$_a$.** At w_a (=0.67 wt %) the dispersion stiffens into a glasslike state. This implies that the interparticle distance in the dispersion has decreased such (below about 200 nm) that the rods are severely hindered in their movement by repulsive double-layer interaction. So, although the particles are nonaggregated, they are immobilized with a preferred orientation (expressed by the birefringence). The particle alignment may for a large part be brought about by flow movement of the dispersion before being at rest, after which the flow texture was "frozen in". An indication that this birefringent glassy phase is a nonaggregated system is the mobility of microscopically small air bubbles observed for a solid content just above w_a. This implies a flow at nearly zero-shear conditions, which seems only possible when the rods have some residual freedom of motion. We call this type of very viscous birefringent dispersion a *glasslike* phase, whereas the term *gel* is restricted to the coagulated (attractive) system.

The visually observed viscoelastic behavior can be explained from the type of dispersion texture, as was done earlier by Larson and Mead[38] who observed similar

(34) Hough, D. B.; White, L. R. *Adv. Colloid Interface Sci.* **1980**, *14*, 3.
(35) Velamakanni, B. V. Ph.D. Thesis, University of California, Santa Barbara, 1990.
(36) Horn, R. G.; Clarke, D. R.; Clarkson, M. T. *J. Mater. Res.* **1988**, *3*, 413.
(37) Israelachvili, J. N. *Intermolecular and surface forces*, 2nd ed.; Academic Press: New York, 1991.
(38) Larson, R. G.; Mead, D. W. *J. Rheol.* **1989**, *33*, 1251.

textures as that in Figure 6 after cessation of shear in liquid crystalline hydroxy propyl cellulose solutions. The director is not uniformly distributed over the whole dispersion but inside small microscopic regions (domains). During flow, this polydomain structure is refined and the particles will align with the direction of shear. When the flow is stopped, the director will slowly vary in both directions out of the shear plane, driven by the accumulated elastic energy. Thereby, the domains will increase in size, resulting in the texture as in Figure 6.

For the dialyzed ASB31 system the experimental $w_a \approx$ 10 wt % seems disproportionately high compared to that of the ASBIP8 system. Apparently, the short rods of ASB31 with their extended, more spherical double layers exhibit insufficient double-layer overlap to form an aligned glassy phase at a low volume fraction.

The observed phase separation of the monophasic birefringent ASBIP8 glassy phase upon salt addition is explained by the compression of the diffuse double layer. The extension of the repulsion decreases, and w_a shifts to a higher value. As a consequence, the boehmite concentration of the dispersion enters the region where the particles have enough mobility for phase separation to take place.

Calculation of the I–N Transition. The permanently-birefringent ASBIP8 glassy phase seems to be a metastable frozen-in state. It is interesting to compare its volume fraction with the fraction ϕ_n at which Onsager's theory[10] predicts a monophasic nematic dispersion. According to the Onsager approach for a system of N *hard* rods in a volume V, the dimensionless particle concentration c_n, where the biphasic isotropic + nematic region is left and a monophasic nematic results (I–N transition), is given by[39]

$$c_n = \frac{\pi}{4} L^2 D \frac{N}{V} = 4.2 \tag{19}$$

Here, L is the rod length and D its diameter. The corresponding volume fraction of cylindrical hard rods is given by

$$\phi_n = \frac{\pi}{4} L D^2 \frac{N}{V} = 4.2 \frac{D}{L} \tag{20}$$

So for a hypothetical uncharged ASBIP8 system, ϕ_n may be as large as 21%. In our case of *charged* rods, eq 19 becomes

$$c_n = \frac{\pi}{4} L^2 D_{eff} \frac{N}{V} = 4.7 \tag{21}$$

Here, D_{eff} is the effective diameter due to the surrounding double layer. We have taken into account the influence of the twist effect which results according to ref 12 in a higher c_n of 4.7 (see the calculated twist parameter after eq 27). The volume fraction is now

$$\phi_n = 4.7 \frac{D^2}{L D_{eff}} \tag{22}$$

The effective diameter is determined by the interparticle distance where the repulsive energy due to overlap of the outer parts of the diffuse double layers is of the order of kT.[10] For the interaction energy between two cylinders a large distance apart, the expression for stiff, infinitely-long polyelectrolytes can be used in the far-field form[32,40,41]

$$\frac{w^{el}}{kT} = \frac{A' \exp(-\kappa(x - D))}{\sin \gamma} \tag{23}$$

with

$$A' = \frac{\pi \Gamma^2 \exp(-\kappa D)}{2\kappa Q} \tag{24}$$

In these equations, x is the shortest distance between the rod axes, γ is their mutual angle, and $Q = 0.714$ nm is the Bjerrum length in water at 298 K. The factor Γ is the proportionality constant in the expression for the electric potential in the outer region from the surface (far-field), where for $e\psi/kT < 1$ the Poisson–Boltzmann equation is solvable and yields the linearized Debye–Hückel version

$$\Psi = \Gamma K_0(R) \tag{25}$$

Here, $\Psi = e\psi/kT$ and $R = \kappa r$ are the dimensionless potential and distance from the cylinder axis, respectively. K_0 is the modified Bessel function of the second kind of zeroth order.

In the inner region of the double layer ($e\psi/kT > 1$), the Debye–Hückel approximation severely underestimates the real potential value, which is given by the nonlinear Poisson–Boltzmann equation. The value of Γ for the outer region, in which we are interested, will depend on this potential behavior in the inner region. Philip and Wooding[42] provided a method to determine Γ by iteratively adjusting the potentials in the inner and outer regions to each other.

The expression for D_{eff} follows from the derivation of the second virial coefficient (which incorporates eq 23) and is given by Onsager[10] as

$$D_{eff} = D + \kappa^{-1}[\ln A' + C_E + \ln 2 - 1/2] \tag{26}$$

where $C_E = 0.5772 \ldots$ is Euler's constant.

For the dialyzed ASBIP8 dispersion (see Table 1) we can derive from ref 42 the proportionality constant $\Gamma = 1.70$. Substitution of $A' = 118$ in eq 26 gives

$$D_{eff} = D + 5.54\kappa^{-1} \tag{27}$$

Thus, according to eq 22 with $D_{eff} = 180$ nm, we find a volume fraction $\phi_n \approx 1.8\%$ and, using a boehmite density of 3.01 g cm^{-3},[43] a w_n of 5.2 wt %, that is nearly 8 times larger than the experimental w_a (0.67 wt %). The twist parameter amounts $h = (\kappa D_{eff})^{-1} = 0.16$. As was found by Fraden et al.[11] for TMV rods, the Onsager theory for charged rods severely overestimates ϕ_n in the case of low ionic strength, especially in the case of a high polydispersity in the rod length.[39,45] In spite of this, the calculations seem to confirm that, far before the concentration is reached where the I–N transition may take place to form a stable nematic phase, the particles are already immobilized by strongly repulsive double-layer interaction in such a way that they form a glassy phase with ordered regions.

Dominating Attractive Interactions. Above an ionic strength of 0.05 M there is insufficient double-layer screening of the van der Waals attraction between the boehmite rods. As a result the rods are immobilized by sticking together in an open three-dimensional network of connected particles. An equivalent critical ionic strength

(39) Lekkerkerker, H. N. W.; Coulon, P.; van der Haegen, R.; Deblieck, R. *J. Chem. Phys.* **1984**, *80*, 3427.
(40) Brenner, S. L.; Parsegian, V. A. *Biophys. J.* **1974**, *14*, 327.
(41) Fixman, M.; Skolnick, J. *Macromolecules* **1978**, *11*, 863.
(42) Philip, J. R.; Wooding, R. A. *J. Chem. Phys.* **1970**, *52*, 953.
(43) Wilson, S. J.; Stacey, M. H. *J. Colloid Interface Sci.* **1981**, *82*, 507.
(44) Scheele, R. B.; Lauffer, M. A. *Biochemistry* **1967**, *6*, 3076.
(45) Kajiwara, K.; Donkai, N.; Hiragi, Y.; Inagaki, H. *Makromol. Chem.* **1986**, *187*, 2883.

for gelation of 6.5×10^{-2} M NaCl was found earlier by Gieselmann et al.[46] for a different type of (sol–gel prepared) boehmite. Obviously, the ionic strength needed to induce coagulation does not depend on the shape of the particles. Gels formed in this interaction regime by particles sticking together are more stiff than the birefringent glassy phase in the repulsive regime.

The compression of the gel by expulsion of solvent can have several causes which may operate at the same time. Firstly, a network of open flocks may collapse under gravity. Secondly, the network may show syneresis: shrinkage of the ramified gel structure due to the formation of extra interparticle bonds. As was observed experimentally, a dispersion of short rods is able to form a more dense network than a system of long needlelike particles.

Apparently the rods, though coagulated, are able to rearrange themselves. It is suggested[47] that a hydration layer, which causes a strong repulsive force at very short interparticle distances (~1 nm) may act as a "lubricant" by which the coagulated particles are able to move. This might explain the weak birefringence in the settled ASB31 gel as follows. The rods coagulate in a random orientation, after which they slowly rearrange to a more parallel orientation, which is the energetically more stable situation. This will be more easily done in the short particle system because these particles have less linkages per particle in the gel.

Further Discussion. Until now the boehmite surface is assumed to be homogeneously covered with surface groups. For crystalline materials, however, different crystal planes may show differing trends in acidity, adsorption density, specific ion adsorption, and so on. For instance, Van Olphen[48] explained the high viscosity of dilute dispersions of kaolinite clay particles by sticking together of oppositely-charged particle faces and edges.

A strong indication for charge inhomogeneity at the boehmite surface is that the overall charge density on the particle found with potentiometric titration is much lower than the theoretical hydroxyl-site density of the boehmite basal plane found in literature. Probably, crystal faces other than the basal one have a lower charge density. The crystal structure of boehmite (γ-AlOOH) is built up of double sheets of octahedra of Al ions surrounded by O and OH groups,[49] with interlayers in between. The boehmite rods are elongated parallel to these sheets, which gives them their flattened shape. The hydroxyl density on the basal (010) plane of the stack of octahedral sheets is much higher than that at its sides. Therefore, the rods are indeed expected to have a higher surface-charge density on their flat sides than on the other sides. As a consequence, the double-layer geometry would not be cylindrical but that of a flattened cylinder. As κ^{-1} increases, the double layer will become increasingly cylindrical.

Another nonideal property of boehmite is the possibility of swelling in water. Like with clay minerals, the octahedral sheets may be pushed apart by adsorption of water molecules in the interlayers. This way, the particle volume can increase several orders of magnitude and the same holds for the effective boehmite volume fraction.

Acknowledgment. DSM Research, Geleen, The Netherlands, is thanked for the use of their electrophoresis apparatus and Petri Mast for the assistance with the measurements.

(46) Gieselmann, M. J.; Anderson, M. A. *J. Am. Ceram. Soc.* **1989**, *72*, 980.
(47) Homola, A. M.; Israelachvili, J. N.; Gee, M. L.; McGuiggan, P. M. *J. Tribol.* **1989**, *111*, 675.
(48) Olphen, H. van *Discuss. Faraday Soc.* **1951**, *11*, 82; *Introduction to Clay Colloid Chemistry*; Interscience: New York, 1963.
(49) Deer, W. A.; Howie, R. A.; Zussman, J. *An Introduction to the Rock-Forming Minerals*; Longman Group Limited: Harlow, 1966.